Radiation Physics and Chemistry 200 (2022) 110427

Contents lists available at ScienceDirect

Radiation Physics and Chemistry

journal homepage: www.elsevier.com/locate/radphyschem

Development of a methodology for dose optimization in abdominal exams using two computed radiography (CR) systems

M.P.S. Alves [a,*], B.P. Mota [a], E.M. Policarpo [a], T.S. Jornada [a], L.P.F. Assemany [b], K.A.C. Daros [a,**]

[a] Universidade Federal de São Paulo - Departamento de Diagnóstico por Imagem da Escola Paulista de Medicina da UNIFESP, Rua Napoleão de Barros, 800 - Vila Clementino, CEP 04024-002, São Paulo, SP, Brazil

[b] Instituto de Pesquisas Energéticas e Nucleares, IPEN – CNEN/SP, Av. Prof. Lineu Prestes, 2242, Cidade Universitária, 05508-000, São Paulo, SP, Brazil

1. Introduction

When acquiring images, regarding ALARA principle, the patient dose is controlled by the X ray (XR) spectrum system settings, control of scattered radiation and detector efficiency to acquire the digital image. The acquisition techniques (AT) settings result in the XR beam spectrum. This spectrum is adjusted by the operator who can select the kilovoltage (kV) of the XR tube, the product of tube current and exposure time (mAs), the XR tube filtration and, the geometric parameters as beam collimation and source-to-image distance (SID) (Seibert, 2008; Bushong, 2020).

The replacement of the screen-film system by digital image systems, as computed radiography (CR), the visual ability to distinguish under-exposed or overexposed images was reduced (Oh et al., 2021; Seibert, 2008). ln computerized radiography, as the CR used in this study, the contrast-to-noise ratio (CNR) and noise levels (N) as AT function can be metrics parameter to analyze image quality (IQ) and its low and high resolution results. Therefore, this metric can promote the optimization of the doses (Young et al., 2006; Hess and Neitzel, 2012).

The goal of this study is to propose a methodology to optimize the Abd_R entrance skin kerma (ESK), performed by different ATs using polymethyl methacrylate (PMMA) phantom, two combinations of CR and XR equipment, CNR and N metrics and IQ resolution tools.

2. Methodology

The study took place at Universidade Federal de São Paulo (UNIFESP), within the Department of Diagnostic Image of its Medical Hospital School – Hospital São Paulo (HSP).

The images were performed in two systems, referred as A and B: Different CRs manufacturers CR-A and CR-B and two different XR equipment, Siemens®, Axion Iconos MD, with additional filter of 1.0 mmAl and the Philips®, Compact Plus, with additional filter of 1.55 mmAl, respectively. All systems under institutional Quality Control Program. The characteristic of the system combination and image plates (IP) of the CR's and image matrix (rows and columns) can be seen on Table 1.

2.1. Methodology steps

- *Step 1: Optimization*

To both systems (A and B), different AT were adjusted and modified by the experience of a radiologic technologist. To simulate a typical adult abdominal, ten PMMA phantom of the 30 × 30 cm^2 and 2 cm thickness, with 0.5 mm Al in the middle of the PMMA (Hariyati et al., 2019). Each ATs was repeated three times to promote statistical analysis, totalizing 396 images in raw data.

The kV and mAs used in the study are in Fig. 1. The SID was 1.2 m, distance usually applied in Abd_R and collimation field of 30x30 cm^2.

The 396 images CNR was used as indicator of image quality. CNR was evaluated by two regions of interest (ROI) with ~5 cm^2 placed in the image, one at projected aluminum contrast object and one beside it (in PMMA). An example of this method is in Fig. 2.

To estimate the ESK, a calibrated detector Radcal®, model 10X6-06 and an electrometer model 2068 were used on the PMMA phantom. To estimate ESK, 396 exposures were performed.

The CNR was calculated by equation (1) (Young et al., 2006; Hess and Neitzel, 2012):

$$CNR = \frac{\overline{PV_1} + \overline{PV_2}}{\sqrt{\frac{1}{2}\left(SD_1^2 + SD_2^2\right)}} \quad (1)$$

where, $\overline{PV_1}$ is the average of the pixel value of the PMMA, $\overline{PV_2}$ is the average of the pixel value of the Al, SD_1 is the standard deviation of the

* Corresponding author.
** Corresponding author.
E-mail addresses: alves.marcos@unifesp.br (M.P.S. Alves), daros.kellen@unifesp.br (K.A.C. Daros).

https://doi.org/10.1016/j.radphyschem.2022.110427
Received 25 February 2022; Received in revised form 11 July 2022; Accepted 15 July 2022
Available online 22 August 2022

Table 1
Characteristic of system combination: XR equipment and IPs of the CR's with image matrix (rows and columns).

System		A	B
CR	**IP Material**	BaSr + FBr: Eu	BaF(Br,I): Eu^{2+}
	Rows	4280	4240
	Columns	3520	3480
XR equipment		Siemens®, Axion Iconos MD	Philips®, Compact Plus

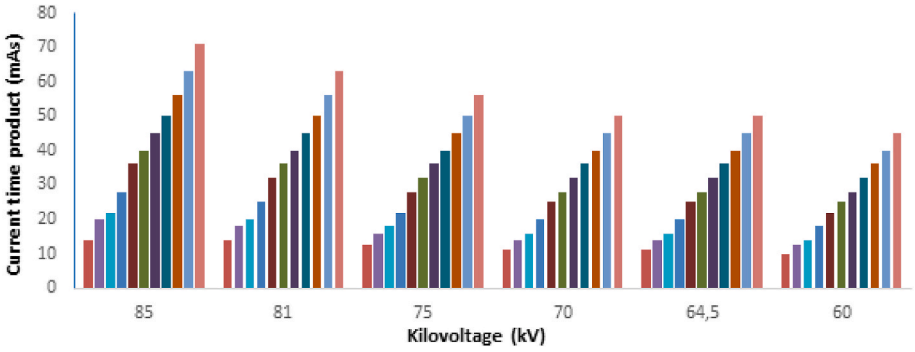

Fig. 1. ATs applied (kV and mAs) for the both systems, A and B.

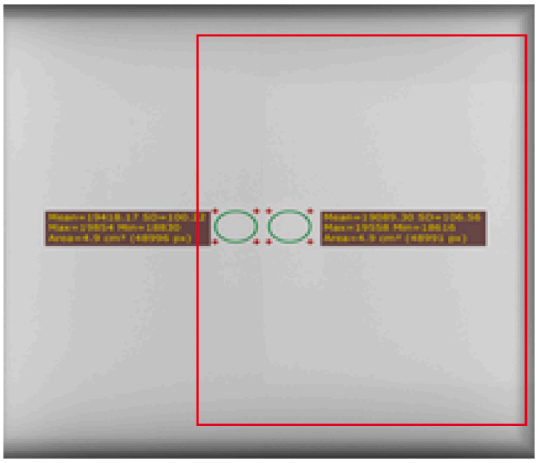

Fig. 2. Inside the red line, there is a typical image for CNR evaluation using two ROI, one on the image of aluminum and another one on PMMA.

pixel mean of the PMMA and SD_2 is the standard deviation of the pixel mean of the Al.

In this study, the SD_1 was the N on the background (PMMA) (Young et al., 2006).

- *Step 2: Evaluation of resolution*

The optimized AT (OAT) from the step 1 results, were defined by intersection between plotted CNR and N as an ESK function. To each OAT three images were performed, totalizing 36 images of 20 cm of PMMA (Fig. 3 A) to evaluate the spatial resolution of the images.

The evaluation of a high and low-contrast spatial resolution, was done with a Shimadzu® tools (Fig. 3B and C) sit in the middle of the PMMA thickness and exposed by OATs.

Two radiologic technologists and two medical physicists analyzed the images using a 3 MP LG display, model 21HK512D.

✓ *Step 2.1: Evaluation of high contrast resolution*

The results of high contrast resolution from the OATs images (Fig. 3A

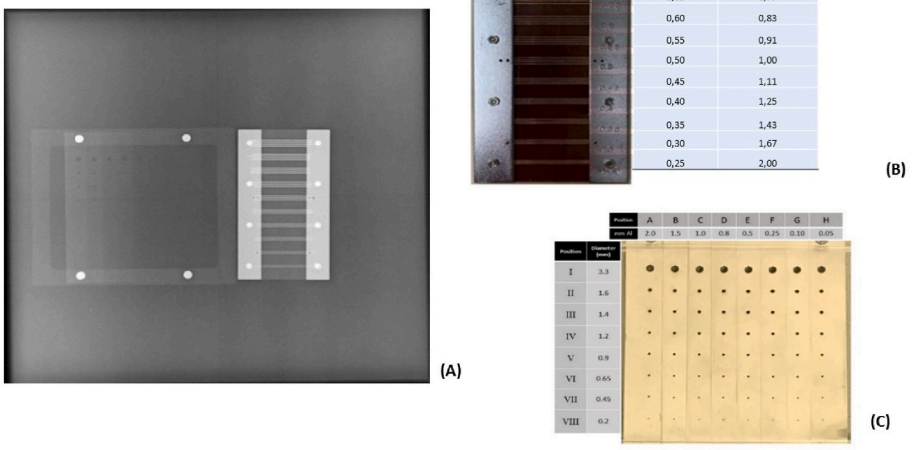

Fig. 3. A. Abd_R images acquired according to the methodology described in step 2, using the high and low contrast resolution tools. **B.** Image of high-contrast resolution tool. **C.** Image of low-contrast resolution tool.

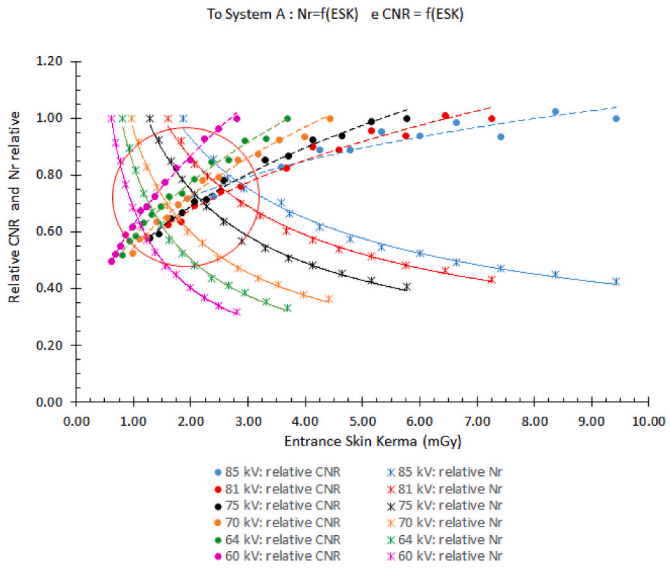

Fig. 4. System A - Intersection between CNR and Nr as function of ESK. The red circle shows the OATs. The error bars in these figures are smaller than 5%.

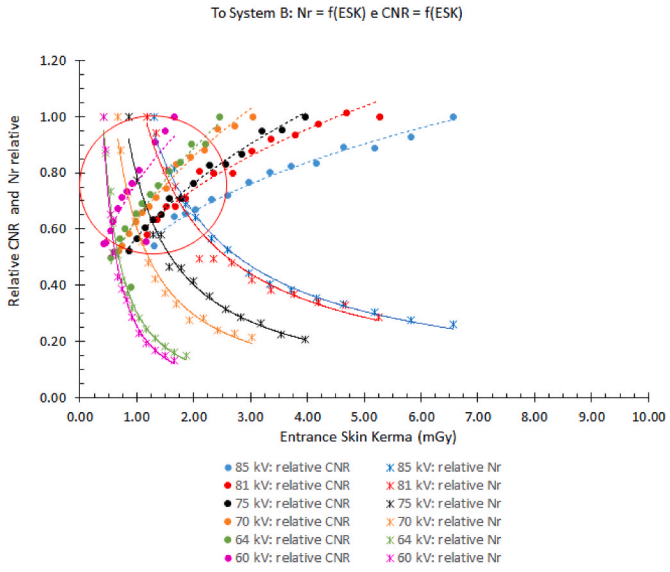

Fig. 5. System B - Intersection between CNR and N as function of ESK. The red circle shows the OATs. The error bars in these figures are smaller than 5%.

and B) were compared from Brazilian regulation that is 2.5 pl/mm (Brasil. Ministério da Saúde, 2021). Only to OATs with results near of the 2.5 pl/mm were evaluated by low contrast resolution (step 2.2).

✓ *Step 2.2: Evaluation of low contrast resolution*

To evaluate low-contrast resolution from the OATs images (Fig. 3A and C) was defined the image quality figure (IQF), calculated by the sum of the products of Al thickness and diameter for the just visible objects in the phantom image (equation (2)), a lower IQF indicates better image quality. Then, the OAT with lower ESK and IQF was considering the final optimized OAT (Tung et al., 2007).

$$IQF = \sum_{i=I}^{n} C_i D_{i,\,th} \tag{2}$$

where I *is* the column number, C_i is Al thickness, and $D_{i,th}$ the threshold diameter (detail) in the column i (Tung et al., 2007)

3. Results and discussion

- Results of Step 1: Optimization

In Figs. 4 and 5 to systems A and B, respectively, the red circle are the OATs results. The error bars in these figures are smaller than 5%. In Table 2 and Table 3, there are the details of the OATs, ESK and curves fit from Fig. 4 e 5.

- *Results of step 2.1: Evaluation of high contrast resolution*

The results of the relative high contrast resolution from OATs images to system A and B are shown in the Fig. 6 and Fig. 7, respectively.

In the Fig. 6, it is seen that OATs 4, 5 and 6 (with higher kV performed), produce a better image quality in terms of the high contrast resolution. The relative high contrast resolution are less than 0.5 because the images are in raw data.

In the Fig. 7, it is seen that all OATs (with any kV performed), produce the same image quality in terms of the high contrast resolution. As system A, the relative high contrast resolution are less than 0.5 because the images are in raw data.

Due the worst results to high contrast from OAT 1, 2 and 3, only to OATs 4 to 12, were evaluated in terms of low contrast resolution (step 3).

- *Results of step 2.2: Evaluation of low contrast resolution*

The results of relative IQF (RIQF), to OATs of systems A and B, are in Figs. 8 and 9, respectively. The values were normalized to lower IQF, so

Table 2
Detail of the OATs from Fig. 4, to systems A.

OAT	Kilovoltage (kV)	Current x time (mAs)	EKS (mGy)	*Curve fit* $\mathbf{CNR_r}$[a]		*Curve fit* $\mathbf{N_r}$[b]	
				equation	R^2	equation	R^2
1	60	18	1.12	$y = 0.6239x^{0.4759}$	0.99	$y = 0.6839x^{-0.772}$	0.99
2	64	18	1.33	$y = 0.5796x^{0.4154}$	0.99	$y = 0.8348x^{-0.732}$	0.99
3	70	18	1.59	$y = 0.5449x^{0.4151}$	0.99	$y = 0.9579x^{-0.678}$	0.99
4	75	22	2.27	$y = 0.5285x^{0.3804}$	0.99	$y = 1.1412x^{-0.610}$	0.99
5	81	23	2.53	$y = 0.5362x^{0.3333}$	0.97	$y = 1.1412x^{-0.549}$	0.99
6	85	21	2.63	$y = 0.6132x^{0.2344}$	0.89	$y = 1.3349x^{-0.522}$	0.99

[a] CNR_r, relative CNR.
[b] N_r, relative N.

Table 3
Detail of the OATs from Fig. 5, to systems B.

OAT	Kilovoltage (kV)	Current x time (mAs)	EKS (mGy)	*Curve fit CNR_r*[a]		*Curve fit N_r*[b]	
				equation	R^2	equation	R^2
7	60	15	0.62	$y = 0.7644x^{0.3889}$	0,69	$y = 0,2548x^{-1.474}$	0.99
8	64	16	0.78	$y = 0.6379x^{0.4774}$	0,78	$y = 0,3038x^{-1.304}$	0.99
9	70	16	0.97	$y = 0.6318x^{0.4425}$	0,99	$y = 0,6052x^{-1.035}$	0.98
10	75	18	1.20	$y = 0.5701x^{0.4184}$	0,99	$y = 0,7899x^{-0.975}$	0.98
11	81	22	1.87	$y = 0.5751x^{0.366}$	0,97	$y = 1,1177x^{-0.848}$	0.97
12	85	22	2.03	$y = 0.5246x^{0.3371}$	0,98	$y = 1,1718x^{-0.833}$	0.99

[a] CNRr, relative CNR.
[b] Nr, relative N.

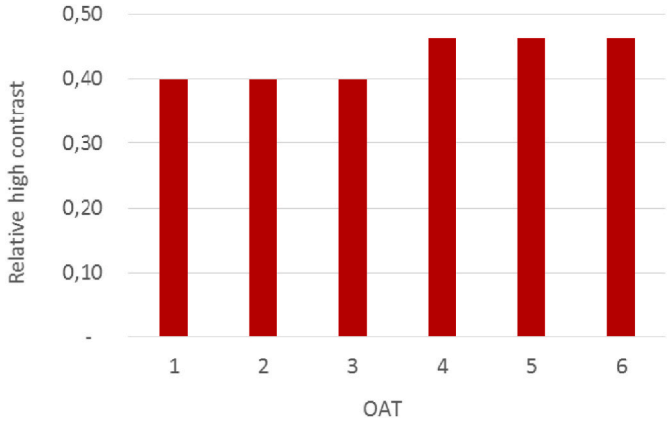

Fig. 6. System A - results of the relative high contrast resolution from OATs images.
The error bars are smaller than 2%.

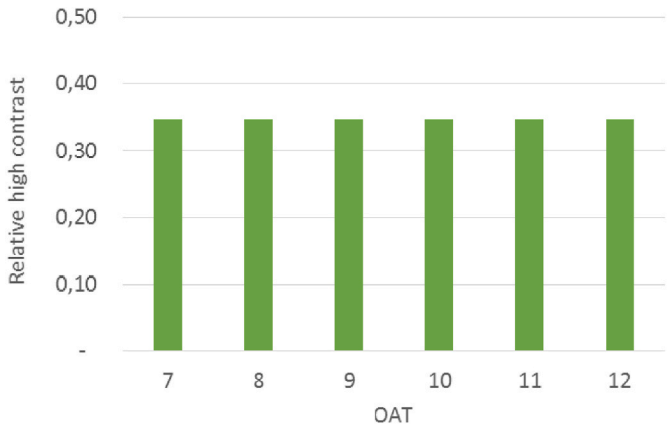

Fig. 7. System B - results of the relative high contrast resolution from OATs images.
The error bars are smaller than 2%.

the better result is near to 1. To system A, Fig. 8, the OAT 5 and 6 presented the best RIQF results. To system B, the best RIQF results were OATs 11 and 12, Fig. 9. The best OAT was defined by lower ESK, Table 4.

In Table 4, there are a summarized data to RIQF to each OAT for both systems (A and B).

4. Conclusion

The methodology was suited to both CR systems. For System A the optimal technique is 81 kV and 23 mAs (ESK = 2.53 mGy). For System B the optimal technique is 81 kV and 22 mAs (ESK = 1.87 mGy). The

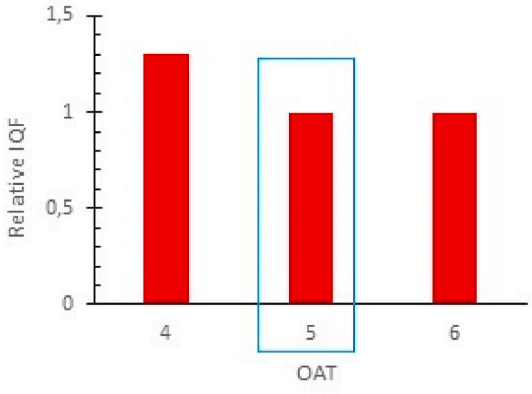

Fig. 8. To system A, results of relative low contrast resolution based on IQF to OATs. The blue line rectangle indicated the best results (low dose with low RIQF).

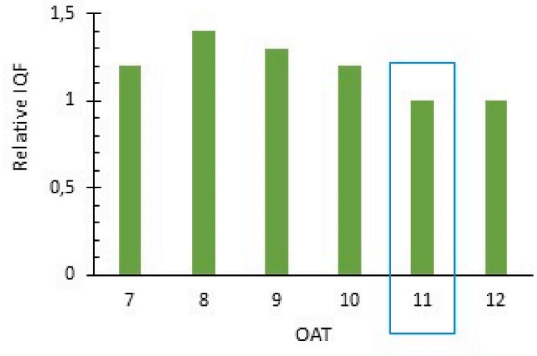

Fig. 9. To system B, results of relative low contrast resolution based on IQF to OATs. The blue line rectangle indicated the best results (low dose with low RIQF).

Table 4
Summarized data to RIQF to each OAT exposure parameters. In gray, the indication of selected OAT.

	OAT	Kilovoltage (kV)	Current x time (mAs)	EKS (mGy)	*Relative IQF*
System A	4	75	22	2.27	1.3
	5	81	23	2.53	1.0
	6	85	21	2.63	0.9
System B	7	60	15	0.62	1.2
	8	64	16	0.78	1.4
	9	70	16	0.97	1.3
	10	75	18	1.20	1.2
	11	81	22	1.87	1.0
	12	85	22	2.03	1.0

optimized doses from System A and System B represent 20% and 18%, respectively, of the maximum reference limit value of the Brazilian regulation (10 mGy).

Considering that the System A is the system used at HSP to clinical application and the ESK average for a typical adult abdominal radiography is 3.5 ± 1.2 mGy (values obtained by the institutional quality assurance program), this study can provide a reduction of 27% on ESK abdominal radiographs.

Author statement

ALVES, M. P. S.: Methodology, Validation, Investigation, Writing original draft.

MOTA B. P.: Data curation.

POLICARPO E. M.: Data Curation.

JORNADA T. S.: Conceptualization.

ASSEMANY, L.P.F.: Formal analysis, Writing - Reviewing and Editing.

DAROS, K. A. C.: Supervision, Funding acquisition, Visualization.

Declaration of competing interest

The authors declare that they have no known competing financial interests or personal relationships that could have appeared to influence the work reported in this paper.

Data availability

The data that has been used is confidential.

Acknowledgement

The authors would like to acknowledge the “Fundação Instituto de Pesquisa e Estudo de Diagnóstico por Imagem” for the operational support and the service department of the “Shimadzu do Brasil” for the supplying the high and low contrast tools.

References

Brasil. Ministerio da Saude. Agencia Nacional de Vigilancia Sanitaria. Radiodiagnostico Medico: Desempenho de Equipamento e Seguranca. IN. No 90 27 maio, 27, 2021. Brasilia: Editora ANVISA.

Bushong, S.C., 2020. Radiologic Science for Technologists E-Book: Physics, Biology, and Protection. Elsevier Health Sciences.

Hariyati, I., Hani, A.D.F., Craig, L.A., Lestariningsih, I., Lubis, L.E., Soejoko, D.S., 2019, June. Optimization of digital radiography system using in-house phantom: preliminary study. In: Journal of Physics: Conference Series, vol. 1248. IOP Publishing. No. 1, p. 012021.

Hess, R., Neitzel, U., 2012, July. Optimizing image quality and dose for digital radiography of distal pediatric extremities using the contrast-to-noise ratio. In: RöFo-Fortschritte auf dem *Gebiet der Röntgenstrahlen und der bildgebenden Verfahren*, vol. 184. © Georg Thieme Verlag KG, pp. 643–649. No. 07.

Oh, S., Kim, J.H., Yoo, S.Y., Jeon, T.Y., Kim, Y.J., 2021. Evaluation of the image quality and dose reduction in digital radiography with an advanced spatial noise reduction algorithm in pediatric patients. Eur. Radiol. 31 (12), 8937–8946.

Seibert, J.A., 2008. Digital radiography: image quality and radiation dose. Health Phys. 95 (5), 586–598.

Tung, C.J., Tsai, H.Y., Shi, M.Y., Huang, T.T., Yang, C.H., Chen, I.J., 2007. A phantom study of image quality versus radiation dose for digital radiography. Nucl. Instrum. Methods Phys. Res. Sect. A Accel. Spectrom. Detect. Assoc. Equip. 580 (1), 602–605.

Young, K.C., Cook, J.J., Oduko, J.M., 2006, June. Automated and human determination of threshold contrast for digital mammography systems. In: International Workshop on D*igital Mammography*. Springer, *B*erlin, Heidelberg, pp. 266–272.